Chinese Physics Letters

EXPRESS LETTER

Thermal Signatures of the Slater–Mott Crossover in the Hubbard Model: From Double Occupancy to Antiferromagnetic Correlation Length

Cite as: Mingzhong Lu *et al*. 2026 *Chin. Phys. Lett.* **43** 110702

DOI CSTR

Recommended Articles

From Ferromagnet to Antiferromagnet: Dimensional Crossover in (111) $SrRuO_3$ Ultrathin Films
Zhaoqing Ding *et al*.
Chin. Phys. Lett. **42**, 120709 (2025)

Thermal Entropy, Density Disorder, and Antiferromagnetism of Repulsive Fermions in 3D Optical Lattice
Yu-Feng Song, Youjin Deng, and Yuan-Yao He
Chin. Phys. Lett. **42**, 110710 (2025)

Flat Band and η-Pairing States in a One-Dimensional Moiré Hubbard Model
R. Wang, and Z. Song
Chin. Phys. Lett. **41**, (2024)

Interplay between the Pseudogap and Superconductivity in Doped Mott Insulators: a Cluster Dynamical Mean-Field Theory Study
Jinbin Liu, Dao-Xin Yao, and Wei Wu
Chin. Phys. Lett. **42**, 080711 (2025)

Breathing-Driven Metal-Insulator Transition in Correlated Kagome Systems
Qingzhuo Duan, Zixuan Jia, Zenghui Fan, Runyu Ma, Jingyao Meng, Bing Huang, and Tianxing Ma
Chin. Phys. Lett. **42**, 090712 (2025)

Parameter-Dependent Superconducting Transition Temperature in a Sign-Problem-Free Bilayer Model
Runyu Ma, Zenghui Fan, Tianxing Ma, and Congjun Wu
Chin. Phys. Lett. **42**, 110705 (2025)

A series journal of Chinese Physical Society distributed by IOP Publishing

Chinese Physics Letters

Chin. Phys. Lett. **43** 110702 (2026)

EXPRESS LETTER

DOI: 10.1088/0256-307X/43/11/110702
CSTR: 32039.14.0256-307X.43.11.110702

Thermal Signatures of the Slater–Mott Crossover in the Hubbard Model: From Double Occupancy to Antiferromagnetic Correlation Length

Mingzhong Lu(卢明忠)[1,2], Yu-Feng Song(宋育峰)[2,3], Youjin Deng(邓友金)[1,3,4,*], and Yuan-Yao He(何院耀)[2,5,6,4,*]

[1]Department of Modern Physics, University of Science and Technology of China, Hefei 230026, China
[2]Institute of Modern Physics, Northwest University, Xi'an 710127, China
[3]Hefei National Laboratory for Physical Sciences at Microscale and Department of Modern Physics, University of Science and Technology of China, Hefei 230026, China
[4]Hefei National Laboratory, Hefei 230088, China
[5]Shaanxi Key Laboratory for Theoretical Physics Frontiers, Xi'an 710127, China
[6]Fundamental Discipline Research Center for Quantum Science and Technology of Shaanxi Province, Xi'an 710127, China

[*]Corresponding authors. Email: yjdeng@ustc.edu.cn; heyuanyao@nwu.edu.cn

The interaction-driven crossover from a Slater insulator to a Mott insulator in the Néel-ordered ground state of the Hubbard model is a fundamental paradigm of strongly correlated electrons, yet its quantitative characterization has remained elusive. Here we establish a clear and experimentally accessible thermal criterion for this crossover via the sign change of the temperature derivative of double occupancy, $(\partial D/\partial T)_U$, near zero temperature. In the Slater regime, $(\partial D/\partial T)_U > 0$ reflects the major role of charge fluctuations; in the Mott regime, the anomalous $(\partial D/\partial T)_U < 0$, a manifestation of the Pomeranchuk effect, signals the dominance of low-energy spin superexchange physics. Using exact diagonalization and numerically exact quantum Monte Carlo simulations, we demonstrate that this criterion determines the crossover boundary at $U_{\mathrm{cross}}/t = 4.0(2)$ for the half-filled two-dimensional Hubbard model. Furthermore, we obtain a consistent boundary independently from the maximum in the antiferromagnetic correlation length, which also arises from the superexchange physics. These two thermal signatures are theoretically unified through the local minimum of thermal entropy versus interaction U at low temperatures. Our results offer a direct, measurable, and physically intuitive framework to identify the Slater–Mott crossover in optical lattice experiments.

The interplay between the Fermi surface geometry and electron–electron interactions is central to strongly correlated electron systems [1–3]. In the Hubbard model [4–6] with nested Fermi surfaces, an infinitesimal repulsion opens a single-particle gap and induces Néel antiferromagnetic (AFM) long-range order in two and three dimensions (2D and 3D) [7–9], rendering the ground state an AFM insulator for any $U > 0$. However, the underlying mechanism of this insulating state changes fundamentally as U increases. At weak coupling, the insulating behavior arises from Fermi surface nesting and weak Néel AFM order, with substantial charge fluctuations, defining the Slater insulator [10]. At strong coupling, charge fluctuations are suppressed and the low-energy physics is controlled by superexchange between local moments [11], which characterize the Mott insulator [12,13]. These two regimes are connected by a smooth crossover [2,3,14,15], whose quantitative and precise characterization remains a considerable challenge.

Existing studies of the Slater–Mott crossover are rather limited and fall into two broad categories. The first approach relies on the distinct spectral features in the Slater and Mott regimes [15–18]. They include the fine and delicate structures in the single-particle spectral function obtained from approximate theories or numerical methods [15–17]. These features, however, often lack a clear criterion for locating the crossover. In addition, linearly extrapolating the spectral gap (i.e., $\Delta_{\mathrm{sp}} \propto U$) [18] captures only the physics deep in the Mott regime. A second approach examines the energetics of the Hubbard model to infer the crossover [17,19–22]. Most of these studies focus on contrasting temperature variations of kinetic and potential energies at weak and strong interactions, within dynamical mean-field theory [17,19–21] in the context of the false Mott metal–insulator transition [23], where the quantitative reliability remains limited. Similarly, a recent diagrammatic Monte Carlo study [22] associates the Slater insulator with a negative temperature derivative of the kinetic energy. Nevertheless, it is restricted to weak and intermediate interactions, and the connection to the ground state is not clarified. While insightful, these prior studies are largely qualitative and have limited applicability to both various theoretical methods [7,8] and optical lattice experiments [24–30]. A simple, quantitatively controlled, and experimentally accessible criterion for the Slater–Mott crossover is therefore still missing.

In this Letter, we establish such a criterion based on the sign of the temperature derivative of double occupancy, $(\partial D/\partial T)_U$. Near $T = 0$, it is positive in the Slater regime and negative in the Mott regime. We validate this criterion using two complementary numerical methods: exact diagonalization (ED) on small systems to reveal the microscopic origin of the sign change, and large-scale auxiliary-field quantum Monte Carlo (AFQMC) simulations to obtain highly precise results of D on extended systems. From the latter, we determine the Slater–Mott crossover boundary at $U_{\mathrm{cross}}/t = 4.0(2)$ for the 2D Hubbard model. Via the Maxwell relation, the sign change in $(\partial D/\partial T)_U$ is linked to the local minimum in thermal entropy $s(U)$, which marks the strongest AFM spin correlations. This link provides an independent determination of the crossover through the maximum of the AFM correlation length $\xi(U)$ at low temperatures, yielding a consistent estimate of the crossover boundary.

We study the half-filled 2D Hubbard model on square lattice described by

$$\hat{H} = \sum_{k\sigma} \varepsilon_{\boldsymbol{k}} \hat{c}^{\dagger}_{k\sigma} \hat{c}_{k\sigma} + U \sum_{i} \left(\hat{n}_{i\uparrow} \hat{n}_{i\downarrow} - \frac{\hat{n}_{i\uparrow} + \hat{n}_{i\downarrow}}{2} \right), \tag{1}$$

where $\boldsymbol{k} = (k_x, k_y)$ is the momentum (lattice constant $a = 1$), and

Received 18 June 2026; accepted 28 September 2026; published 20 October 2026

© 2026 Chinese Physical Society and IOP Publishing Ltd. All rights, including for text and data mining, AI training, and similar technologies, are reserved.

Check for updates

$\hat{n}_{i\sigma} = \hat{c}^{\dagger}_{i\sigma}\hat{c}_{i\sigma}$ (with $\hat{n}_i = \hat{n}_{i\uparrow} + \hat{n}_{i\downarrow}$) is the density operator on the site $\boldsymbol{i}$ with σ ($\uparrow$ or $\downarrow$) denoting spin. The kinetic energy dispersion is $\varepsilon_{\boldsymbol{k}} = -2t(\cos k_x + \cos k_y)$ with t as nearest-neighbor hopping strength (set as the energy unit), and U is the on-site repulsion. This model has nested Fermi surfaces and an AFM insulating ground state for any $U > 0$, but remains paramagnetic at finite T due to the Mermin–Wagner theorem [32]. We solve this model by employing ED (Lanczos algorithm) [33–36] and both ground-state and finite-temperature AFQMC methods [37–50], bridging zero- and finite-temperature properties. In AFQMC simulations, we use supercells with $N_s = L^2$ lattice sites (L the linear system size), and apply periodic and twist-averaged boundary conditions (PBC and TABC), where the latter can reduce finite-size effects in computed observables [51–54]. When applying TABC, we practically take ∼30 sets of twisted angles to achieve well-converged statistics. Additional algorithmic details of AFQMC methods are provided in the Supplemental Material (SM).

From a physical perspective, although the total particle number $\hat{N} = \sum_i \hat{n}_i$ is conserved in the model (1), the local density $\hat{n}_i$ is not a conserved quantity, since $[\hat{H}, \hat{n}_i] \neq 0$. Hence, the local charge density can exhibit quantum fluctuations even in the ground state, despite the presence of a gapped single-particle spectrum and vanishing charge compressibility [31]. These fluctuations constitute an intrinsic part of the charge fluctuations in the system. Such local charge fluctuations can be quantitatively characterized by the local charge variance, which is related to the double occupancy $D = N_s^{-1}\sum_i \langle \hat{n}_{i\uparrow}\hat{n}_{i\downarrow}\rangle$ via $N_s^{-1}\sum_i \langle (\hat{n}_i - n)^2\rangle = 2D$, with $n = N_s^{-1}\langle \hat{N}\rangle = 1$ at half filling. Thus, D serves as a direct and quantitative metric of local charge fluctuations in the model (1). As U/t increases, the monotonically decreasing D in the half-filled Hubbard model [31,45,46] directly reflects the progressively suppressed charge fluctuations.

At finite temperatures, as U/t increases, the model (1) undergoes a smooth metal–insulator crossover (MIC) [22,31,55] from a Fermi liquid first to a bad metal and then to a quasi-AFM insulator, reproduced from Ref. [31] and shown as the background of Fig. 1. An important feature of this MIC is the nonmonotonic U-dependence of thermal entropy density $\boldsymbol{s} = S/N_s$ (in units of k_B) [31,45,46]. In Fig. 1 inset (a), we plot representative results of $\boldsymbol{s}(U)$ at $T/t = 0.2$. While the local maximum in $\boldsymbol{s}(U)$ identifies the crossover from the Fermi liquid to bad metal [31], its subsequent local minimum at $U = U_S$ essentially signals the dominance of the spin superexchange physics at low temperatures [31,45,46]. Moreover, the Maxwell relation

$$\left(\frac{\partial \boldsymbol{s}}{\partial U}\right)_T = -\left(\frac{\partial D}{\partial T}\right)_U \tag{2}$$

reveals that the U_S curve corresponds to the temperature line on which the double occupancy $D(T)$ (at fixed U/t) exhibits a local minimum, denoted as T_D. Based on this relation, figure 1 inset (b) provides an alternative determination of U_S via $(\partial \boldsymbol{s}/\partial U)_T = 0$, which translates into $(\partial D/\partial T)_U = 0$ and yields a U_S value consistent with that in inset (a). We then extrapolate the low-temperature signatures of T_D (see Fig. 3) and U_S to $T = 0$ and obtain the Slater–Mott crossover boundary at $U_{cross}/t = 4.0(2)$. Hence, the $\boldsymbol{s}(U)$ results combined with Eq. (2) establish the crossover criterion near $T = 0$: $(\partial D/\partial T)_U > 0$ for the Slater regime and $(\partial D/\partial T)_U < 0$ for the Mott regime. The T_D and U_S data (summarized in the SM) and their linear fit (red dashed line), along with the crossover criterion, are presented in Fig. 1. Other fitting functions tested produce crossover boundaries that clearly conflict with the $D(T)$ results from AFQMC (see Fig. 3).

Associating the sign change of $(\partial D/\partial T)_U$ with the Slater–Mott crossover is rooted in its connection to Mott–Heisenberg physics, motivated by two insights. First, in the $T < T_D$ (or $U > U_S$) region of Fig. 1, $(\partial D/\partial T)_U < 0$, known as the Pomeranchuk effect [31,45,46,56–59], originates from the virtual hopping [31,45,46], which is the microscopic mechanism underlying spin superexchange [11]. Second, via Eq. (2), the sign change is linked to the local minimum U_S in $\boldsymbol{s}(U)$. Near U_S in the quasi-AFM insulator regime, the charge entropy is negligible and the total entropy is thus dominated by the spin sector [31]. This signals a dip in spin entropy, indicating the strongest

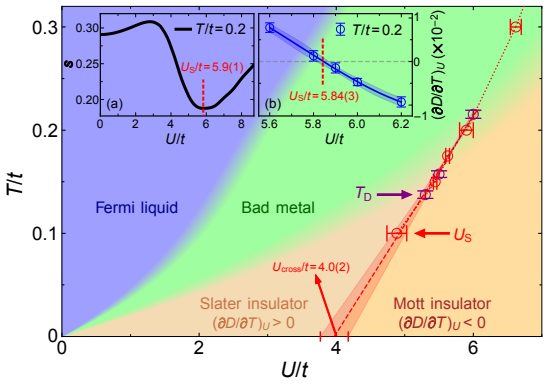

Fig. 1. Extrapolation of the thermal signatures at low temperatures to $T = 0$ yields $U_{cross}/t = 4.0(2)$ as the Slater–Mott crossover boundary for the half-filled square-lattice Hubbard model. The signatures include the local minimum U_S in thermal entropy density $\boldsymbol{s}(U)$ at fixed T/t and the minimum T_D of double occupancy $D(T)$ at fixed U/t (see Fig. 3), which are connected via the Maxwell relation in Eq. (2). A linear fit (red dashed line) to the data is used with the red shaded region indicating the fitting uncertainty. The characteristic feature for the Slater (Mott) regime is $(\partial D/\partial T)_U > 0$ [$(\partial D/\partial T)_U < 0$] near $T = 0$. The background reproduces the finite-T metal–insulator crossover diagram [31], separating the Fermi liquid (blue), bad metal (green), and quasi-AFM insulator (yellow). Inset (a) plots $\boldsymbol{s}(U)$ at $T/t = 0.2$, which exhibits a local minimum at $U_S/t = 5.9(1)$. Inset (b) alternatively determines U_S via $(\partial D/\partial T)_U = 0$ by applying Eq. (2), giving $U_S/t = 5.84(3)$.

AFM spin correlations around $U = U_S$ [31]. For larger U, these correlations are suppressed by the weakened superexchange coupling $J = 4t^2/U$ and the elevated T/J (at fixed T/t) within the effective Heisenberg model [11]. Thus, these insights justify interpreting the extrapolated U_{cross} in Fig. 1 as the crossover boundary.

We next show how the sign of $(\partial D/\partial T)_U$ near $T = 0$ distinguishes between Slater and Mott physics, based on ED analysis on a 4×4 system with PBC. The double occupancy is given by $D(T) = \sum_\ell D_\ell e^{-\beta E_\ell}/\sum_{\ell'} e^{-\beta E_{\ell'}}$ with $\beta = 1/k_B T$, where E_ℓ and $|\phi_\ell\rangle$ are the energy and wavefunction of the ℓ-th eigenstate (and $\ell = 0$ labels the ground state), and $D_\ell = \langle \phi_\ell | N_s^{-1}\sum_i \hat{n}_{i\uparrow}\hat{n}_{i\downarrow}|\phi_\ell\rangle$. We find that all degenerate eigenstates involved in our ED calculations share the same D_ℓ, and that the ground state is nondegenerate for any $U > 0$. For simplicity, we denote g_m as the degeneracy of the m-th excited state ($m \geq 1$), with the eigenenergy E_m. At low temperatures, the summations over ℓ and ℓ' in $D(T)$ can be truncated when $\beta(E_{M+1} - E_0) \gg 1$, as the higher excited states are thermally suppressed, yielding (see details in the SM)

$$D(T) \approx D_0 + \frac{\sum_{m=1}^{M} g_m (D_m - D_0) e^{-\beta(E_m - E_0)}}{1 + \sum_{m'=1}^{M} g_{m'} e^{-\beta(E_{m'} - E_0)}}, \tag{3}$$

where D_m and D_0 are the double occupancy of the m-th excited state and the ground state, respectively. This equation illustrates that, provided $D_m > D_0$ holds for all involved excited states ($1 \leq m \leq M$), then one obtains $D(T) > D_0$ and $(\partial D/\partial T)_U > 0$ [and conversely, $D_m < D_0$ leads to $D(T) < D_0$ and $(\partial D/\partial T)_U < 0$]. It is more evident from the approximation of Eq. (3) near $T = 0$ as $D(T) \approx D_0 + \sum_{m=1}^{M} g_m (D_m - D_0) e^{-\beta(E_m - E_0)}$ (see SM).

In ED, we verify that for $T/t \leq 0.05$, $M = 3$ in Eq. (3) is sufficient to produce accurate results of $D(T)$ across $4 \leq U/t \leq 12$ in the model (1). As depicted in Fig. 2, the $(D_m - D_0)$ results clearly demonstrate the aforementioned behaviors of $D_m > D_0$ for $U/t \leq 6$ and $D_m < D_0$ for $U/t \geq 7$. In the small-U regime, the observed hierarchy $D_m > D_{m-1} > \cdots > D_0$ reveals that, with increasing m, the low-lying excited states possess enhanced charge redistribution compared to the ground state. Since D directly quantifies the charge fluctuations, these results indicate that the low-lying excitations contributing to the thermal variation of D [i.e., $D(T)$] have a predominantly charge-like character. This characterization does not imply the absence of spin

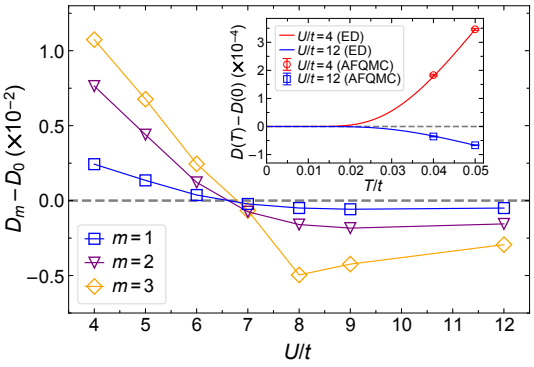

Fig. 2. ED results of $(D_m - D_0)$ as a function of U/t with $m = 1, 2, 3$ on a 4×4 periodic supercell for the model (1), where D_m and D_0 are the double occupancy of the m-th excited state and the ground state, respectively. The inset plots the difference $[D(T) - D(T = 0)]$ versus T/t with $T/t \le 0.05$, from both ED [solid lines, with $D(T)$ computed via Eq. (3)] and AFQMC (circles and squares) for $U/t = 4$ and 12, with $D(T = 0) = D_0$ taken from ED.

excitations in the Slater regime. Instead, the Néel AFM order in this regime also supports collective spin excitations, including transverse spin-wave and longitudinal spin-amplitude fluctuations, which are generally intertwined with charge fluctuations, as discussed in Ref. [60]. By contrast, in the large-U regime, $D_m < D_0$ is characteristic of spin-like excitations. Here, charge fluctuations become strongly suppressed, and $D_0 \propto (t/U)^2$ at ground state [61] arises from the virtual hopping [11]. In low-lying excited states, spin-flip processes create ferromagnetic bonds (in Fock-state basis), which suppress such virtual hopping and thus reduce double occupancy, leading to $D_m < D_0$. Higher spin excitations typically involve more spin flips, rendering $D_m < D_{m-1} < \cdots < D_0$, as indeed observed in Fig. 2. These understandings are consistent with low-energy spin superexchange physics in the Mott regime.

The results in Fig. 2, combined with Eq. (3), illustrate that $(\partial D/\partial T)_U > 0$ for $U/t \le 6$, and $(\partial D/\partial T)_U < 0$ for $U/t \ge 7$. To further examine these behaviors, we compute $D(T)$ via Eq. (3) using (g_m, E_m, D_m) from ED (see SM) and compare with finite-T AFQMC results for $U/t = 4$ and 12, as shown in Fig. 2 inset. The nice agreement between the two methods validates the ED results of $D(T)$. As expected, the $D(T)$ curves evidently confirm the predicted sign of $(\partial D/\partial T)_U$, i.e., positive for $U/t = 4$ and negative for $U/t = 12$. Together, these results and the analyses above establish the connection between the sign of $(\partial D/\partial T)_U$ and the Slater versus Mott regimes via the distinct properties of low-lying excited states. They also provide a direct explanation for the Pomeranchuk effect of $D(T)$ in the Mott regime [31,45,46,56–59]. Quantitatively, the ED results for the $L = 4$ system in Fig. 2 locate the Slater–Mott crossover at $U/t = 6 \sim 7$, which is substantially larger than $U_{\rm cross}/t = 4.0(2)$ found in Fig. 1, a discrepancy we confirm as arising from finite-size effects (see SM).

To access larger systems and accurately determine the low-T behavior of $D(T)$, we turn to large-scale AFQMC with TABC. As indicated by $[D(T) - D(T = 0)]$ results in Fig. 3(a), $D(T)$ increases upon heating for $U/t = 3.5$, signaling $(\partial D/\partial T)_U > 0$ and the Slater regime. In contrast, for $U/t = 4.5$ and 4.75, $D(T)$ decreases with temperature near $T = 0$, rendering $(\partial D/\partial T)_U < 0$ and thus indicating the Mott regime. At $U/t = 4.0$, $D(T)$ instead remains almost constant within statistical uncertainties from $T = 0$ up to $T/t = 0.06$. This near-constancy indicates that $U/t = 4.0$ lies close to the crossover boundary, in agreement with the $U_{\rm cross}/t$ identified in Fig. 1. With increasing U/t deeper into the Mott regime, the $(\partial D/\partial T)_U < 0$ behavior near $T = 0$ becomes more pronounced, as shown in Fig. 3(b). Moreover, $D(T)$ develops a local minimum at $T_{\rm D}$, which is linked via Eq. (2) to the local minimum in $s(U)$ at $U_{\rm S}$. We extract $T_{\rm D}/t = 0.138(4)$, 0.157(3), and 0.215(4) for $U/t = 5.3$, 5.5, and 6.0, respectively, as presented in Fig. 1. Additionally, from Fig. 3(a), we find $T_{\rm D}/t \simeq 0.06$ for $U/t = 4.5$ and $T_{\rm D}/t \simeq 0.09$ for $U/t = 4.75$, both consistent with the red shaded region in Fig. 1, thus supporting the validity of the linear fit.

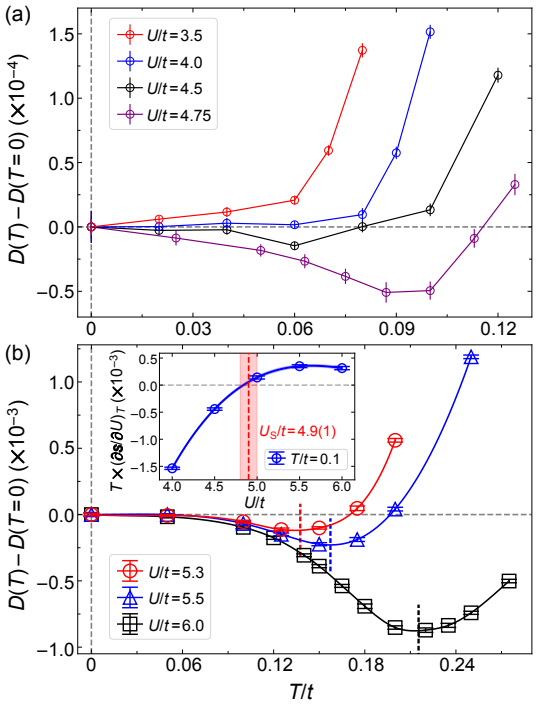

Fig. 3. AFQMC results of $[D(T) - D(T = 0)]$ as a function of T/t obtained under TABC to reveal the Slater–Mott crossover. Panel (a) presents the results around the crossover, and (b) shows those in the Mott regime, with the solid lines as polynomial fits to the data. In (b), the vertical dashed lines mark the local minimum of $D(T)$ at $T_{\rm D}/t = 0.138(4)$, 0.157(3), and 0.215(4) for $U/t = 5.3$, 5.5, and 6.0, respectively. The inset of (b) plots $T\times(\partial s/\partial U)_T$ versus U/t at $T/t = 0.1$ (see text). The $T = 0$ and $T > 0$ results are accordingly computed using ground-state and finite-temperature AFQMC with $L = 20$, and exhibit negligible finite-size effects.

Besides extracting $T_{\rm D}$ from $D(T)$, one can also determine the sign change of $(\partial D/\partial T)_U$, based on Eq. (2), using the local minimum position $U_{\rm S}$ of the entropy $s(U)$. We evaluate $U_{\rm S}$ using three approaches. The first is to explicitly compute $s(U)$ at fixed T/t [45,46,62] and extract $U_{\rm S}$, as shown in Fig. 1 inset (a). However, this method becomes inefficient at low T since $s(U)$ vanishes as $T/t \to 0$. A second approach is to obtain $U_{\rm S}$ from the condition $(\partial s/\partial U)_T = 0$, which is equivalent to $(\partial D/\partial T)_U = 0$. The latter can be directly measured in AFQMC using $(\partial D/\partial T)_U = \beta^2(\langle \hat{H}\hat{D}\rangle - \langle \hat{H}\rangle\langle \hat{D}\rangle)$ (see SM) with the operator $\hat{D} = N_{\rm s}^{-1}\sum_i \hat{n}_{i\uparrow}\hat{n}_{i\downarrow}$. As illustrated in Fig. 1 inset (b), this yields a $U_{\rm S}$ that closely matches that from the first approach. We also find that such a determination of $U_{\rm S}$ exhibits rather weak finite-size effects (see SM), despite the use of $L = 8$ in Fig. 1 inset (b) compared to $L = 20$ in Fig. 1 inset (a). The third approach instead applies $T\times(\partial s/\partial U)_T = (\partial e/\partial U + 1/2) - D(U)$ [with $e(U)$ as total energy density, see SM] to solve $(\partial s/\partial U)_T = 0$ numerically, as depicted in Fig. 3(b) inset. These techniques are used jointly to generate the $U_{\rm S}$ data points, which, combined with the $T_{\rm D}$ data obtained in Fig. 3(b), extrapolate to $U_{\rm cross}/t = 4.0(2)$ at $T = 0$ in Fig. 1.

The sign change of $(\partial D/\partial T)_U$, as previously analyzed, is essentially connected to the strongest AFM spin correlation, which also offers key insight into the Slater–Mott crossover. This correlation is dominated by its long-range part at low T and is characterized by the AFM correlation length ξ. Practically, ξ can be computed from spin structure factor $S_{zz}(\boldsymbol{q}) = \sum_{\boldsymbol{r}} e^{i\boldsymbol{q}\cdot\boldsymbol{r}} C(\boldsymbol{r})$ with the spin correlation $C(\boldsymbol{r}) = N_{\rm s}^{-1}\sum_i \langle \hat{s}_i^z \hat{s}_{i+\boldsymbol{r}}^z\rangle$ [with $\hat{s}_i^z = (\hat{n}_{i\uparrow} - \hat{n}_{i\downarrow})/2$] using $\xi = [2\sin(\pi/L)]^{-1}\sqrt{S_{zz}(\boldsymbol{\pi})/S_{zz}(\boldsymbol{\pi}+\delta\boldsymbol{q}) - 1}$ [45,46], where the momenta $\boldsymbol{\pi} = (\pi,\pi)$ and $\delta\boldsymbol{q} = (2\pi/L, 0)$ or $(0, 2\pi/L)$. In Figs. 4(a)–4(c), we show AFQMC results of ξ versus U/t at $T/t = 0.3$, 0.2, and 0.1, respectively.

At fixed T/t, ξ increases with U/t at weak coupling due to Fermi surface nesting and decreases at strong coupling owing to the reduced $J \propto 1/U$ and the correspondingly elevated T/J within the Heisenberg

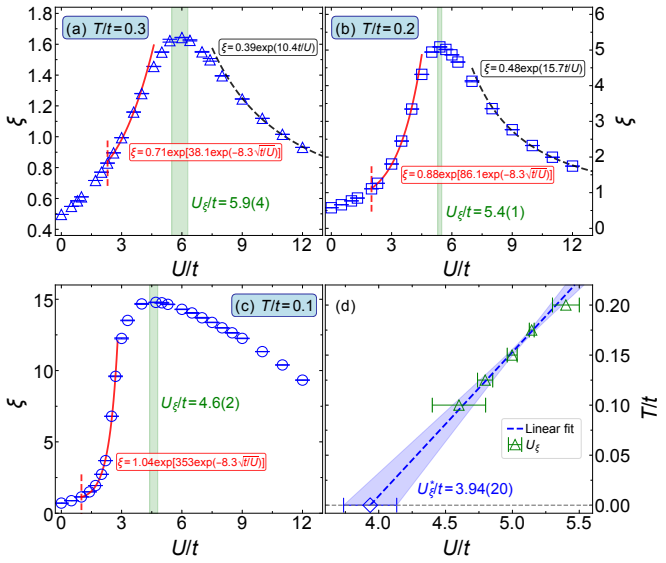

Fig. 4. AFQMC results for the AFM correlation length ξ obtained under PBC, together with the extrapolation of its maximum position to $T = 0$. Panels (a)–(c) present ξ as a function of U/t at $T/t = 0.3$, 0.2, and 0.1, respectively, with $L = 20$ used in (a) and (b), and $L = 24$ in (c). The position of the maximum, denoted U_ξ/t, is indicated by the green shaded band, with the corresponding value included. At weak-coupling side, the ξ data are fitted to $\xi \sim \exp[A\exp(-B\sqrt{t/U})]$ (red solid lines) for all three temperatures, with the starting point of the fit marked by the red dashed line. At strong coupling, the data are fitted to $\xi \sim \exp(Ct/U)$ (black dashed lines) for $U/t \geq 9$ at $T/t = 0.3$ and 0.2. Panel (d) shows the extracted U_ξ/t at different temperatures and its linear extrapolation for $T/t \leq 0.175$, yielding $U^*_\xi/t = 3.94(20)$ at $T = 0$, with the blue shaded region indicating the fitting uncertainty.

model. This gives rise to a maximum in $\xi(U)$, with its location denoted as U_ξ. Upon cooling, the distinct Slater versus Mott mechanisms result in a more pronounced asymmetry of ξ about $U = U_\xi$, as observed in Figs. 4(a)–4(c). Moreover, the U dependence of ξ at both sides can be analyzed at a quantitative level. For the 2D model (1), below a characteristic temperature T_X/t, ξ is expected to display an exponential form $\xi(T) \sim e^{\alpha/T}$ for any fixed U/t [16,63–66], with α being a U-dependent constant. At weak coupling, α is governed by $\Delta_{sp} \sim t\exp(-2\pi\sqrt{t/U})$ [9,67] as the single-particle gap. It leads to $\xi(U) \sim \exp[A\exp(-B\sqrt{t/U})]$ at fixed T/t, which is only valid for $U_0 \lesssim U \lesssim U_1$ with U_0 defined by $T_X(U_0) = T$ and U_1 marking the breakdown of above asymptotic expression of Δ_{sp}. At $T/t = 0.2$, Ref. [63] obtained $U_0/t \simeq 2$, which should be smaller (larger) at $T/t = 0.1$ ($T/t = 0.3$). This is incorporated in the fit of $\xi(U)$ below U_ξ (red solid line), as shown in Figs. 4(a)–4(c). At strong coupling, α is instead set by $J = 4t^2/U$ [66], which yields $\xi(U) \sim \exp(Ct/U)$ at fixed T/t. Our $\xi(U)$ data support such scaling for $U/t \geq 9$ at $T/t = 0.3$ and 0.2, with the extracted C agreeing well with a $1/T$ form, as seen from the fit (black dashed line) in Figs. 4(a) and 4(b). Finite-size effects in $\xi(U)$ are noticeable around U_ξ (absent at $T/t = 0.3$, small at 0.2, significant at 0.1), while U_ξ itself converges rapidly for the system sizes used. Notably, at $T/t = 0.1$, the maximal ξ (~ 15) and its values at $9 \leq U/t \leq 12$ remain comparable to $L/2$ of the $L = 24$ system [see Fig. 4(c)], indicating that ξ is cut off by the finite system size. Such significant finite-size effects depend on U/t, and therefore prevent a meaningful fit to the asymptotic exponential form for the $\xi(U)$ data.

Near $U \sim U_\xi$, where J and T/J exhibit little variation, the rapid suppression of $\xi(U)$ once $U > U_\xi$ is instead attributed to the high-order frustrating interactions in the effective spin model [11]. These include the next-nearest-neighbor and ring-exchange couplings, both $\propto 1/U^3$. The long-range AFM spin correlation is highly vulnerable to such frustrations, which causes ξ to decrease. Thus, U_ξ at low T signals the onset of spin superexchange. We note that the peak in $\xi(U)$ and the sign change of $(\partial D/\partial T)_U$ (or the entropy minimum at U_S) are not directly related. Instead, they are two independent thermal manifestations of the same underlying crossover: the emergence of spin-superexchange dominated physics once charge fluctuations are sufficiently suppressed. While the entropy minimum at U_S indicates similar physics, we find U_ξ is consistently slightly smaller than U_S at the same T/t (see SM). This is because U_S reflects the overall AFM spin correlations and is therefore less sensitive to frustrations than ξ is. This discrepancy gradually vanishes as $T/t \to 0$, when long-range AFM correlations dominate. Hence, extrapolating U_ξ to $T = 0$ should independently determine the Slater–Mott crossover boundary. We perform this procedure in Fig. 4(d) using a linear fit to the U_ξ/t data, reaching $U^*_\xi/t = 3.94(20)$. This value is in nice agreement with $U_{cross}/t = 4.0(2)$ from Fig. 1, thus providing compelling support for our physical picture of the crossover and the Slater versus Mott mechanisms.

All the above physical interpretations and calculations can be readily applied to a group of Hubbard models hosting the Slater–Mott crossover, including the 2D modified model with spin-nematic hopping [68,69], the bilayer model [70–72], the SU($2N$) models (for instance $N = 2$ and 3) [18,73–75], and the 3D model on simple cubic lattice [45,46,76]. In particular, for the half-filled 3D Hubbard model, we obtain $U^{3D}_{cross}/t = 5.7(2)$ as the crossover boundary from the analysis of AFM correlation length (see SM). Our numerical results also have implications for optical lattice experiments [24–30], which have now entered the low-T regime ($T/t \sim 0.05$) [25] of the Hubbard model and can directly measure both double occupancy [29] and AFM correlation length [24]. Moreover, recent double occupancy measurements have achieved a precision better than 0.1% and serves as a decisive indicator of lattice superfluidity [77]. Given these capabilities and further improvements, future optical lattice experiments should be able to resolve the $D(T)$ and $\xi(U)$ results in Figs. 3 and 4, thereby directly visualizing the Slater–Mott crossover.

We then briefly comment on other physical observables that are related to the Slater and Mott physics in the half-filled Hubbard model. The local moment is directly tied to D as $\langle m_z^2\rangle = N_s^{-1}\sum_i\langle(\hat{n}_{i\uparrow} - \hat{n}_{i\downarrow})^2/4\rangle = 1/4 - D/2$ [78], and its low-T derivative would exhibit an opposite sign-change behavior to $(\partial D/\partial T)_U$, thus offering a similar criterion for the Slater–Mott crossover. The charge compressibility χ_e [31] is strictly zero at $T = 0$ for the insulating ground state, and $(\partial\chi_e/\partial T)_U > 0$ near $T = 0$ holds for any $U > 0$ [22], providing no distinction between the two regimes. The uniform spin susceptibility χ_s exhibits a similar behavior, with $(\partial\chi_s/\partial T)_U > 0$ near $T = 0$ for any $U > 0$ [22,79]. As for the kinetic energy e_K, our high-precision AFQMC results explicitly show $(\partial e_K/\partial T)_U > 0$ in the low-T regime across the crossover (see SM), which does not support a clear criterion. These observations reinforce that our proposed criterion based on the sign change of $(\partial D/\partial T)_U$ is a direct, highly physically relevant, and experimentally accessible marker of the Slater–Mott crossover.

In summary, we have established a simple and quantitative thermal criterion for the Slater–Mott crossover in the Hubbard model in terms of the temperature dependence of double occupancy near $T = 0$, i.e., $(\partial D/\partial T)_U > 0$ in the Slater regime and $(\partial D/\partial T)_U < 0$ in the Mott regime. Using ED calculations, we validate this criterion by linking the sign of $(\partial D/\partial T)_U$ to the low-lying excited state properties characteristic of Slater and Mott physics. We further verify the criterion via low-temperature behavior of $D(T)$ obtained from large-scale AFQMC simulations, and pinpoint $U_{cross}/t = 4.0(2)$ as the crossover boundary for the 2D Hubbard model. Moreover, through the Maxwell relation, the sign change of $(\partial D/\partial T)_U$ is connected to the entropy minimum and, consequently, to the maximum of AFM correlation length, from which we reach a consistent boundary estimate. Beyond locating the crossover, our work offers a direct thermal perspective on the ground-state Slater–Mott crossover that is readily accessible in optical lattice experiments.

Acknowledgments

This work was supported by the National Natural Science Foundation of China (Grant Nos. 12247103, 12204377, and 12275263), the Quantum Science and Technology—National Science and Technology Major Project (Grant No. 2021ZD0301900), the Natural Science Foundation of Fujian province of China (Grant No. 2023J02032), and the Youth Innovation Team of Shaanxi Universities.

References

[1] Georges A, Kotliar G, Krauth W, and Rozenberg M J 1996 *Rev. Mod. Phys.* **68** 13
[2] Imada M, Fujimori A, and Tokura Y 1998 *Rev. Mod. Phys.* **70** 1039
[3] Lee P A, Nagaosa N, and Wen X G 2006 *Rev. Mod. Phys.* **78** 17
[4] Hubbard J 1963 *Proc. R. Soc. London A* **276** 238
[5] Kanamori J 1963 *Prog. Theor. Phys* **30** 275
[6] Gutzwiller M C 1963 *Phys. Rev. Lett.* **10** 159
[7] Arovas D P, Berg E, Kivelson S A, and Raghu S 2022 *Annu. Rev. Condens. Matter Phys.* **13** 239
[8] Qin M, Schäfer T, Andergassen S, Corboz P, and Gull E 2022 *Annu. Rev. Condens. Matter Phys.* **13** 275
[9] Hirsch J E 1985 *Phys. Rev. B* **31** 4403
[10] Slater J C 1951 *Phys. Rev.* **82** 538
[11] Delannoy J Y P, Gingras M J P, Holdsworth P C W, and Tremblay A M S 2005 *Phys. Rev. B* **72** 115114
[12] Mott N F 1949 *Proc. Phys. Soc. A* **62** 416
[13] Mott N F 1968 *Rev. Mod. Phys.* **40** 677
[14] Yang J, Hao L, Meyers D, Dasa T, Xu L, Horak L, Shafer P, Arenholz E, Fabbris G, Choi Y, Haskel D, Karapetrova J, Kim J W, Ryan P J, Xu H, Batista C D, Dean M P M, and Liu J 2020 *Phys. Rev. Lett.* **124** 177601
[15] Pruschke T and Zitzler R 2003 *J. Phys.: Condens. Matter* **15** 7867
[16] Borejsza K and Dupuis N 2003 *EPL* **63** 722
[17] Fratino L, Sémon P, Charlebois M, Sordi G, and Tremblay A M S 2017 *Phys. Rev. B* **95** 235109
[18] Wang D, Wang L, and Wu C 2019 *Phys. Rev. B* **100** 115155
[19] Gull E, Werner P, Wang X, Troyer M, and Millis A J 2008 *Europhys. Lett.* **84** 37009
[20] Rohringer G and Toschi A 2016 *Phys. Rev. B* **94** 125144
[21] van Loon E G C P, Hafermann H, and Katsnelson M I 2018 *Phys. Rev. B* **97** 085125
[22] Kim A J, Simkovic F, and Kozik E 2020 *Phys. Rev. Lett.* **124** 117602
[23] Schäfer T, Geles F, Rost D, Rohringer G, Arrigoni E, Held K, Blümer N, Aichhorn M, and Toschi A 2015 *Phys. Rev. B* **91** 125109
[24] Mazurenko A, Chiu C S, Ji G, Parsons M F, Kanász-Nagy M, Schmidt R, Grusdt F, Demler E, Greif D, and Greiner M 2017 *Nature* **545** 462
[25] Xu M, Kendrick L H, Kale A, Gang Y, Feng C, Zhang S, Young A W, Lebrat M, and Greiner M 2025 *Nature* **642** 909
[26] Kendrick L H, Kale A, Gang Y, Deters A D, Lebrat M, Young A W, and Greiner M 2025 arXiv: 2509.18075 [cond-mat.quant-gas]
[27] Bourgund D, Chalopin T, Bojović P, Schlömer H, Wang S, Franz T, Hirthe S, Bohrdt A, Grusdt F, Bloch I, and Hilker T A 2025 *Nature* **637** 57
[28] Shao H J, Wang Y X, Zhu D Z, Zhu Y S, Sun H N, Chen S Y, Zhang C, Fan Z J, Deng Y, Yao X C, Chen Y A, and Pan J W 2024 *Nature* **632** 267
[29] Wang Y X, Shao H J, Zhu Y S, Zhu D Z, Sun H N, Chen S Y, Yao X C, Chen Y A, and Pan J W 2025 *Phys. Rev. Lett.* **134** 043403
[30] Chalopin T, Bojović P, Wang S, Franz T, Sinha A, Wang Z, Bourgund D, Obermeyer J, Grusdt F, Bohrdt A, Pollet L, Wietek A, Georges A, Hilker T, and Bloch I 2026 *Proc. Natl. Acad. Sci. U.S.A* **123** e2525539123
[31] Lu M, Song Y F, Deng Y, and He Y Y 2026 *Phys. Rev. B* **113** 195154
[32] Mermin N D and Wagner H 1966 *Phys. Rev. Lett.* **17** 1133
[33] Dagotto E 1994 *Rev. Mod. Phys.* **66** 763
[34] Lin H, Gubernatis J, Gould H, and Tobochnik J 1993 *Comput. Phys.* **7** 400
[35] Prelovšek P and Bonča J 2013 *Ground State and Finite Temperature Lanczos Methods* (Springer, Berlin, Heidelberg) p. 1
[36] Wu H Q, He Y Y, Fang C, Meng Z Y, and Lu Z Y 2016 *Phys. Rev. Lett.* **117** 066403
[37] Blankenbecler R, Scalapino D J, and Sugar R L 1981 *Phys. Rev. D* **24** 2278
[38] Hirsch J E 1983 *Phys. Rev. B* **28** 4059
[39] White S R, Scalapino D J, Sugar R L, Loh E Y, Gubernatis J E, and Scalettar R T 1989 *Phys. Rev. B* **40** 506
[40] Scalettar R T, Noack R M, and Singh R R P 1991 *Phys. Rev. B* **44** 10502
[41] Wu C and Zhang S C 2005 *Phys. Rev. B* **71** 155115
[42] Assaad F and Evertz H 2008 *Computational Many-Particle Physics* (Springer, Berlin, Heidelberg) p. 277
[43] He Y Y, Qin M, Shi H, Lu Z Y, and Zhang S 2019 *Phys. Rev. B* **99** 045108
[44] Sun F and Xu X Y 2024 *Phys. Rev. B* **109** 235140
[45] Song Y F, Deng Y, and He Y Y 2025 *Phys. Rev. Lett.* **134** 016503
[46] Song Y F, Deng Y, and He Y Y 2025 *Phys. Rev. B* **111** 035123
[47] He Y Y 2025 arXiv: 2505.17411 [cond-mat.str-el]
[48] Sugiyama G and Koonin S 1986 *Ann. Phys.* **168** 1
[49] Sorella S, Baroni S, Car R, and Parrinello M 1989 *Europhys. Lett.* **8** 663
[50] Du H and He Y Y 2025 *Phys. Rev. B* **112** 235120
[51] Lin C, Zong F H, and Ceperley D M 2001 *Phys. Rev. E* **64** 016702
[52] Xu H, Chung C M, Qin M, Schollwöck U, White S R, and Zhang S 2024 *Science* **384** eadh7691
[53] Qin M, Shi H, and Zhang S 2016 *Phys. Rev. B* **94** 085103
[54] Vitali E, Shi H, Qin M, and Zhang S 2016 *Phys. Rev. B* **94** 085140
[55] Šimkovic F, LeBlanc J P F, Kim A J, Deng Y, Prokof'ev N V, Svistunov B V, and Kozik E 2020 *Phys. Rev. Lett.* **124** 017003
[56] Gorelik E V, Rost D, Paiva T, Scalettar R, Klümper A, and Blümer N 2012 *Phys. Rev. A* **85** 061602
[57] Li G, Antipov A E, Rubtsov A N, Kirchner S, and Hanke W 2014 *Phys. Rev. B* **89** 161118
[58] Wietek A, Rossi R, Šimkovic F, Klett M, Hansmann P, Ferrero M, Stoudenmire E M, Schäfer T, and Georges A 2021 *Phys. Rev. X* **11** 041013
[59] Li Q, Gao Y, He Y Y, Qi Y, Chen B B, and Li W 2023 *Phys. Rev. Lett.* **130** 226502
[60] Schrieffer J R, Wen X G, and Zhang S C 1989 *Phys. Rev. B* **39** 11663
[61] Avella A, Mancini F, and Saikawa T 2003 *Eur. Phys. J. B* **36** 445
[62] Song Y F, Deng Y, and He Y Y 2026 *Phys. Rev. B* **114** 115101
[63] Schäfer T, Wentzell N, Šimkovic F, He Y Y, Hille C, Klett M, Eckhardt C J, Arzhang B, Harkov V, Le Régent F M C M, Kirsch A, Wang Y, Kim A J, Kozik E, Stepanov E A, Kauch A, Andergassen S, Hansmann P, Rohe D, Vilk Y M, LeBlanc J P F, Zhang S, Tremblay A M S, Ferrero M, Parcollet O, and Georges A 2021 *Phys. Rev. X* **11** 011058
[64] Chakravarty S, Halperin B I, and Nelson D R 1989 *Phys. Rev. B* **39** 2344
[65] Borejsza K and Dupuis N 2004 *Phys. Rev. B* **69** 085119
[66] Beard B B, Birgeneau R J, Greven M, and Wiese U J 1998 *Phys. Rev. Lett.* **80** 1742
[67] Langmann E and Lenells J 2026 *Lett. Math. Phys.* **116** 50
[68] Gukelberger J, Wang L, and Pollet L 2017 *Phys. Rev. B* **95** 205121
[69] Xie Z, Song Y F, and He Y Y 2025 *Phys. Rev. B* **111** 125105
[70] Kancharla S S and Okamoto S 2007 *Phys. Rev. B* **75** 193103
[71] Golor M, Reckling T, Classen L, Scherer M M, and Wessel S 2014 *Phys. Rev. B* **90** 195131
[72] Gall M, Wurz N, Samland J, Chan C F, and Köhl M 2021 *Nature* **589** 40
[73] Cai Z, Hung H H, Wang L, Zheng D, and Wu C 2013 *Phys. Rev. Lett.* **110** 220401
[74] Zhou Z, Cai Z, Wu C, and Wang Y 2014 *Phys. Rev. B* **90** 235139
[75] Wang D, Li Y, Cai Z, Zhou Z, Wang Y, and Wu C 2014 *Phys. Rev. Lett.* **112** 156403
[76] Song Y F, Deng Y, and He Y Y 2025 *Chin. Phys. Lett.* **42** 110710
[77] Private communication with Xing-Can Yao.
[78] Paiva T, Scalettar R T, Huscroft C, and McMahan A K 2001 *Phys. Rev. B* **63** 125116
[79] Moreo A 1993 *Phys. Rev. B* **48** 3380